Sohag Journal of Sciences
An International Journal

AC and DC electrical properties of CuO nanoparticles synthesized using free surfactant hydrothermal method.

Mena P. Monis[*], *A.M. Abdel Hakeem, N.M. Hadia, Hani A.A. Saadallah, E.M.M. Ibrahim*

Physics Department, Faculty of Science, Sohag University, Sohag-82524, Egypt

Received: 3 Jul. 2022, Revised: 31 Jul. 2022, Accepted: 5 Aug. 2022.
Published online: 1 Sep. 2022

Abstract: The electrical conductivity and dielectric behavior of CuO nanoparticles prepared by hydrothermal method without any surfactant and annealed for 2 hours at 350 ^{o}C were studied in the temperature range of 303 K – 403 K and frequency range of 10 – 10^6 Hz. The X-ray diffraction was used for investigating the crystallinity and microstructure and confirmed formation of the single phase monoclinic structure. The surface morphology as well as particle shape and size were investigated using field emission scanning electron microscope (FESEM). The DC electrical measurements reveal that the conductivity (σ_{DC}) increases with increasing the temperature in a typical behavior of the semiconductors. The AC conductivity (σ_{AC}) dependence of temperature is well represented by the Jonscher's power law, $\sigma_{AC} = A\omega^n$. The value of frequency exponent (n) is less than unity indicating that the conduction is governed by the correlated barrier hopping model. The dielectric constant and the dielectric loss increase with the temperature and decrease with frequency. The obtained results nominate the synthesized samples for using in gas sensing and energy storage applications.

Keywords: CuO nanoparticles, Hydrothermal, AC electrical, DC electrical, Dielectric constant, Dielectric loss.

1 Introduction

Last decades, transition metal oxide (TMO) nanostructures have attracted great interest due to their fascinating properties and applications such as gas sensors [1], supercapacitors [2], and piezoelectricity [3]. Preparation of metal oxide nanostructures with particular morphology is a vital requirement for developing new nanodevices with diverse applications.

Copper oxide (CuO) is one of a hot topic studies on TMO because of its interesting properties such as, nontoxicity, inexpensive, abundantly, easy synthesis, low band gap energy (E_g = 1.2 eV), antimicrobial response, superthermal conductivity, colossal magnetoresistivity, high stability, photovoltaic potency, and high-temperature superconductivity [4]. Consequently, CuO based nanomaterial with improved structural, optical and electronic properties have been used in many electronic and optoelectronic devices including photodetectors, solar cells, non-volatile memory devices, gas sensors, etc. [5]. The electrical properties of CuO based-nanomaterials can be tuned by controlling the number of the interfacial atoms and defects in the internal structure where these defect centres have a major role in DC and AC conduction and dielectric properties [6].

In fact, many CuO nanostructures with various morphologies, such as nanocrystals [7], nanocubes [8], nanorods [9], nanowires [10], and nanosheets [11] have been synthesized using several techniques such as; co-precipitation method, sol-gel [12], electrochemical [13], and hydrothermal [14] etc. The results of the experimental studies confirm that the cupric source, concentration, reaction time, temperature and pH value of the precursor medium have significant influence on the growth, morphologies, and particle size of the final subsequent CuO nanostructure which leads to various optical, electrical, and catalytic properties [8]. Hydrothermal technique is heterogeneous reactions for synthesizing inorganic materials in aqueous media at ambient temperature and pressure. It is one of the best techniques for the synthesis of nanoparticles (NPs) where it offers a number of advantages such as low reaction temperature, high porosity to obtain materials with high surface area, and growth of good crystals with controlled stoichiometry. In this study, pure CuO NPs are synthesized using free-surfactant hydrothermal method. The structural and morphological properties are investigated with focusing on the DC and AC electrical properties.

* Corresponding author E-mail: mena.phelobos@gmail.com

2 Experimental Details

2.1. Materials

Copper nitrate trihydrate $[Cu(NO_3)_2.3H_2O]$, and sodium hydroxide [NaOH] were used as the starting materials. deionized water was selected as a solvent in this preparation process. All the chemicals and solvents used were of analytical reagent grade.

2.2. Synthesis of CuO nanostructures

Synthesis of CuO nanostructures by hydrothermal method is generally based on a two-step process:

First, formation of copper hydroxide $[Cu(OH)_2]$ by the reaction of a cupric salt precursor with a basic solution, such as sodium hydroxide (NaOH).

Second, the $Cu(OH)_2$ particles are then thermally dehydrated in an autoclave at a fixed temperature.

To synthesis CuO nanoparticles without any surfactant, at first, 0.025 mol copper nitrate trihydrate was stirred magnetically for 15 min at 50 ^oC to completely dissolve copper nitrate into deionized water. Then NaOH solution was added in drops until reaching pH = 11 with continuous stirring for 30 min at 50 ^oC. The solution was transferred to a teflon lined stainless steel autoclave which was placed in a muffle furnace at 170 ^oC for 24 h. After terminating the reaction, the autoclave was furnace cooled to room temperature. The obtained black precipitate was cleaned with deionized water and ethanol and finally dried at 100 ^oC for 2 h in air, then annealed at 350 ^oC for 2 h.

2.3. Characterization

To investigate the crystal structure of CuO nanoparticles (NPs), the synthesized samples were investigated by x-ray diffractometer (XRD, Bruker D8 Advance) with Cu-Kα radiation source λ = 1.5406 Å, where the XRD patterns were recorded over a diffraction angle (2θ) range from 25° to 80°. Surface morphology and elemental analysis were examined by field emission scanning electron microscope (FESEM, ZEISS Microscopy). The dielectric constant, loss factor, impedance, and AC conductivity were measured using IM 3536 LCR Meter HIOKI.

3 Results and discussion

3.1. Structural analysis

Fig. 1 shows x-ray diffraction pattern of the pure CuO powder sample. The pattern illustrates twelve distinct diffraction peaks at 2θ = 32.5°, 35.4°, 38.6°, 46.15°, 48.58°, 53.3°, 58.20°, 61.4°, 66.1°, 68.0°, 72.2° and 75.1° corresponding to the crystallographic planes (110), (11$\bar{1}$), (111), ($\bar{1}$12), (20$\bar{2}$), (020), (202), ($\bar{1}$13), (31$\bar{1}$), (220), (311) and (004), respectively. All of these peaks characterize pure monoclinic single-phase of CuO in coincidence with the COD (9016105) data of the copper oxide. The values of the lattice parameters a, b, c and β are determined using the following equation [8]:

$$\frac{1}{d^2} = \frac{1}{sin^2\,\beta}\left(\frac{h^2}{a^2} + \frac{k^2\,sin^2\,\beta}{b^2} + \frac{l^2}{c^2} - \frac{2hl\cos\beta}{ac}\right) \quad (1)$$

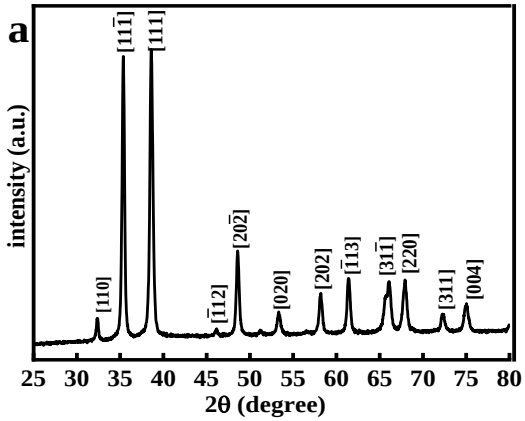

Figure 1. The XRD patterns of CuO.

The values are in a good matching with those of the standard data (see Table1). The sharpness and high intensity of the recorded diffraction peaks indicate a high degree of crystallinity of the samples.

The value of the unit cell volume (V), of the monoclinic system was calculated using the lattice geometry equation [**15**]:

$$V = abc\ sin\,\beta \quad (2)$$

The obtained value (81.507 $Å^3$) matches also with the characteristic value of the CuO monoclinic structure according to the DOC (9016105) card.

The XRD data allow to calculate the crystal size (D) of a material using the well-known Scherers' equation [**15**]:

$$D = \frac{K\,\lambda}{\beta_{hkl}\ cos\,\theta} \quad (3)$$

where k is the shape factor (taken to be 0.9), λ is the wavelength of the incident x-ray beams (1.5406 Å), βhkl is the full width at half maximum (FWHM) corrected for the instrumental broadening of the XRD peaks, and θ is the diffraction angle. Noteworthy, eq. (3) was applied for the most intense diffraction peak (111). As shown in Table 1, the average crystallites size is 39.503 nm. Noteworthy, the XRD peak can be broadened due to the internal stress and defects, so the average crystal size calculated by Scherrers' equation is smaller than the actual value [**16**].

Because of the crystallites are in the nano-sized scale, a large fraction of surface atoms to volume ratio is obtained. These atoms form unsaturated dangling bonds which may cause many unusual chemical and physical properties of materials. Furthermore, an internal crystalline strain is raises and may affect the properties of the materials including the

electronic characteristics [16]. In this study, the internal strain (ε) was estimated using the following relation [**15**]:

$$\varepsilon = \frac{\beta_{hkl}\, cos\, \theta}{4} \qquad (4)$$

The calculated value of ε is found to be 8.774×10^{-4}. The dislocation density (δ) of CuO NPs was calculated to be 6.408×10^{14} line/m2 by using the following relation:

$$\delta = \frac{1}{D^2} \qquad (5)$$

Table 1. The 2θ value, the lattice parameters (a, b, c, a/b, c/b and β), the unit cell volume (V), the crystal size (D), the dislocation density (δ) and the internal strain (ε) of the CuO nanoparticle.

Lattice parameter	Experimental data	Standard data
2θ	38.604	--
a ($A°$)	4.720	4.68
b ($A°$)	3.413	3.42
c ($A°$)	5.131	5.12
a/b	1.383	--
c/b	1.507	-
β	99.567	99.5
$V(A^3)$	81.507	--
$\varepsilon \times 10^{-4}$	8.774	--
D (nm)	39.503	--
$\delta \times 10^{14}$ (line/m^2)	6.408	--

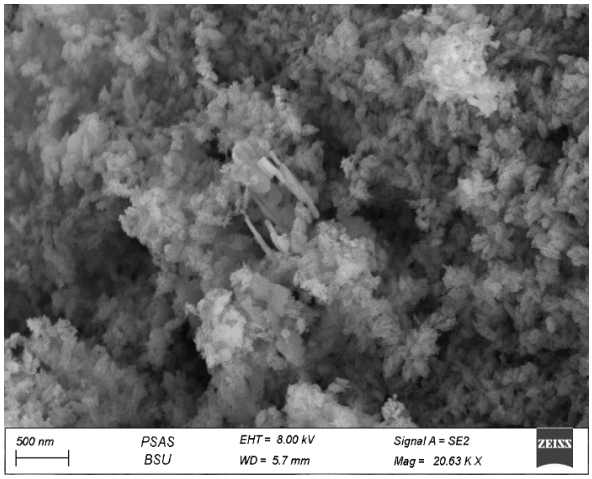

Figure 2. the SEM image of pure CuO.

The surface morphology and particle size distribution of the material under study were investigated by the field emission scanning electron microscope (FESEM) (ZEISS-Sigma 500). Note that, the image depicted in Fig. 2 reveal a large degree of similarity between particles. The sample seems to consist of agglomerated tiny particles with average particle size 60 nm. The particle agglomeration is reasonable because of the large number of the surface atoms which form dangling bonds which in turn make weak bonds between the particles. The average particle size obtained from the FESEM investigation is slightly higher than that obtained from XRD analyses because the role of the crystalline strain that decreases the value calculated by Scherrers' equation.

3.2. The electrical conductivity

The total conductivity can be determined by the following equation:

$$\sigma_{TOT} = \sigma_{AC} + \sigma_{DC} \qquad (6)$$

where the total conductivity σ_{TOT} is the sum of AC conductivity (σ_{AC}) and DC conductivity (σ_{DC}). As there is a finite probability for both types of conduction mechanisms to occur, the relative probabilities depend on many factors such as the energy of charge carriers, the frequency of the applied field, temperature, etc.

3.2.1. The DC conductivity (σ_{DC})

In order to identify the electrical properties of the CuO NPs, DC conductivity (σ_{DC}) was measured as a function of temperature in the temperature range between 300 K and 483 K. Fig. 3 shows Lnσ_{DC} versus 1/T for the NPs. The data reveal that the sample is characterized by a typical semiconductor behavior; where by increasing the temperature, an increasing number of thermally activated charge carriers can overcome the energy barrier and contribute to the electrical conduction. The electrical conductivity of the CuO NPs is higher than that reported for bulk sample due to the higher oxygen vacancy content that accompanies the decrease of the particles to the nanosized scale [**16-18**]. The oxygen vacancies create an intrinsic defect in the CuO sample which in turn present donor states in the forbidden band slightly below the conduction band and hence change the electronic structure of CuO.

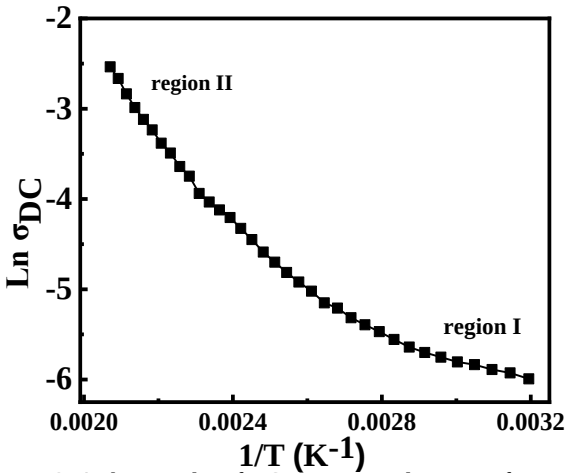

Figure 3. Arrhenius plot of DC electric conductivity of pure and cobalt doped CuO nanomaterial.

The Lnσ_{DC} vs. 1/T plot shown in Fig. 3 consists of two linear parts confirming presence of two thermally activated conduction mechanisms each of them dominates over a specific range of temperature. The conduction mechanisms were found to follow the well-known Arrhenius' equation:

$$\sigma = \sigma_O\, exp\, (-E_a/K_B\, T) \qquad (7)$$

where σ_0 is the pre-exponential factor, Ea is the activation energy of electrical conduction which correspond to the minimum energy required for conduction from one site to another and undergo physical transport, T the absolute temperature, and KB for the Boltzmann constant. The activation energy (Ea) of the DC conductivity is calculated from the slopes of the two linear parts of the ln (σ_{DC}) versus 1/T plot to be 0.127 eV and 0.38 eV for the region I and region II, respectively. The change in the Ea values indicate that the sample exhibits a transition between two different conduction mechanisms with increasing the temperature. The activation energy at low temperature (region I) is possibly a result of existence of the oxygen vacancies ($V_0 \rightarrow V_0^+ + e^-$) while that of the high temperature (region II) can be attributed to desorption of O_2^- species according to the reaction ($O_2^- \rightarrow O_2 + e^-$). In the other word, shallow and deep donor levels are created in the band gap of the CuO NPs. On conclusion, charge carriers are thermally activated from the deep donor levels and shallow donor levels to the conduction band in region II and region I, respectively [16].

3.2.2. AC conductivity (σ_{AC})

Variation of the AC conductivity (σ_{AC}) with frequency (ω) measured at various temperature values from 303 K to 403 K for pure CuO NPs were studied. Fig. 4 shows the corresponding Ln(σ) vs. Ln(ω) plot. Each plot consists of two distinct regions: (I) almost flat or plateau region at the low frequency region characterizing the contribution of the DC conductivity (σ_{DC}) where the conductivity is frequency independent. It is observed that, the width of the σ_{DC} region increases with increasing the temperature. (II) the second region, or namely the dispersion region, characterizes the higher frequency region where the AC conductivity (σ_{AC}) increases with increasing the frequency. The width of dispersion region is observed to decrease with increasing the ambient temperature of measurement. Noteworthy, the total conductivity (σ) increases with temperature due to the increases in the number of the charge carriers and thermal agitation.

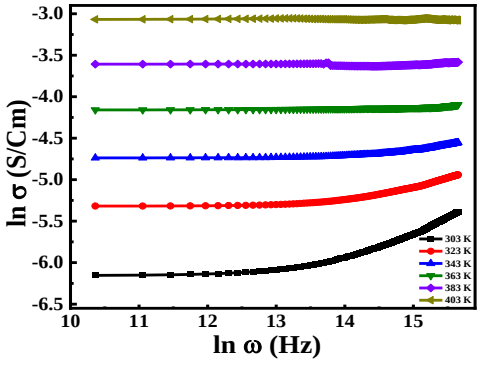

Figure 4. The dependence of AC conductivity on the frequency at different temperature for pure CuO NPs

The frequency dependency of σ_{AC} is represented by Jonscher's universal power law equation:

$$\sigma_{AC} = A\,\omega^n \qquad (8)$$

where (A) is proportionality constant, (ω) is the angular frequency and (n) is the frequency exponent.

The frequency exponent (n) is plotted as a function of temperature, where the value of (n) decreases with increasing the temperature (See Fig. 5) which can be attributed to the increase in the charge carriers density. The n values (tabulated in Table 2) are much less than unity indicating that the conduction mechanism is governed by the Correlated Barrier Hopping (CBH) model where the conductivity of a material is a result of charge carriers hopping between two defect centers.

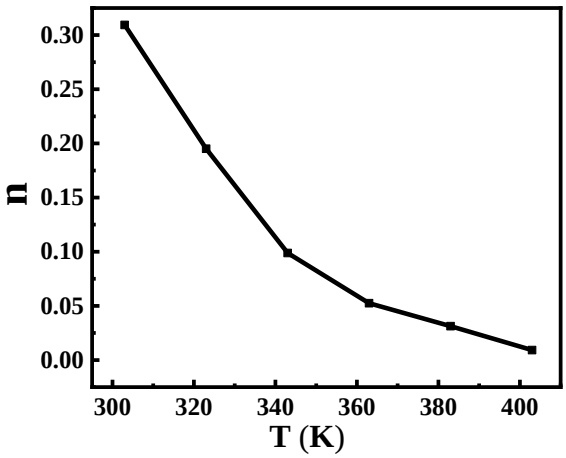

Figure 5. the dependence of frequency exponent (n) with temperature (T) for pure CuO sample.

Table 2: The frequency exponent (n) values of CuO sample determined at different temperatures.

T (K)	*303*	*323*	*343*	*363*	*383*	*403*
n	*0.309*	*0.195*	*0.098*	*0.052*	*0.031*	*0.009*
W_m (eV)	*0.226*	*0.207*	*0.196*	*0.190*	*0.188*	*0.187*

According to the CBH model, the temperature dependency of n is represented by the following question:

$$n = 1 - \frac{6\,K_B\,T}{W_m} \qquad (9)$$

Where Wm is the barrier height at a separation distance, commonly called "the polaron binding energy "and defined as the energy required to move an electron from one site to another site, k_B is Boltzmann constant, and T is the absolute temperature. Where the binding energy (W_m) is given by following equation:

$$W_m = \frac{6\,K_B\,T}{1-n} \qquad (10)$$

It was seen that the binding energy (W_m) decreases with temperature indicating that the hopping distances decreases with increasing the temperature.

3.3. Dielectric constant

The dielectric properties of the materials are characterized by the complex permittivity (ε*) given by the equation:

$$\varepsilon^* = \varepsilon' - j\varepsilon'' \qquad (11)$$

Where ε′ and ε″ are the real and imaginary components of the complex dielectric constant.

3.3.1. Real part of dielectric constant (ε')

The real part of dielectric constant (ε') can be calculated by using the following equation:

$$\varepsilon' = \frac{C\ d}{\varepsilon_o\ A} \qquad (12)$$

where C is the measured capacitance, d is the sample thickness, εo is the dielectric constant in vacuum ($\varepsilon_o = 8.854\ \times 10^{-12}\mathrm{F/m}$), and A is the sample area.

The overall polarizability of a polar material is attributed to the contribution of multi–component polarization mechanisms such as electronic, ionic, space charge and orientational polarization. Each mechanism has its own distinctive feature with varied contribution to the total polarization. The ionic polarization occurred only in dielectric materials with inter-atomic ionic bonds and become effective up to the infrared region. The electronic polarization results from displacement of the electron clouds with respect to their nucleus and it is only effective above the infrared region. Generally, ionic and electronic polarization have no significant contribution to the total polarizability because they are effective in the frequency range of the infrared region or higher. The high value of dielectric constant at low frequencies results from the orientational polarization, which depends on both frequency and temperature [6].

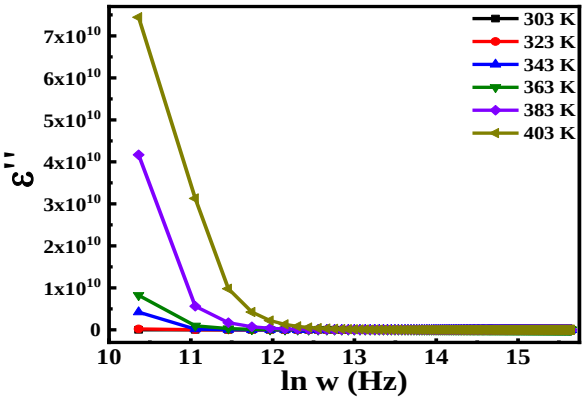

Figure 6. The variation of ε′ with ln (ω) for pure CuO sample at different temperatures.

As an electric field is applied, the molecule rotates to align itself along the field, causing a net average dipole moment per molecule. Also, the material can exhibit an interfacial or space charge polarization due to accumulation of charges at an interface between two regions of different conductivity resulting in formation of dipole moments. Interfacial polarization is commonly observed in amorphous or polycrystalline solids.

Because of their high aspect ratio, nanostructured materials contain large number of interfacial atoms and defects at the grain boundaries compared to bulk materials [19] which can cause positive and negative space charge distribution and generate space charge polarization.

Fig. 6. shows the frequency and temperature dependence of dielectric constant (ε') for the pure CuO NPs. ε' have higher values at low frequencies and decreases exponentially with increasing the frequency. ε' increases with increasing the temperature because, at high temperatures, the bound dipoles gain enough thermal energy and become able to follow the change in the external field more easily, [6].

Existence of oxygen vacancies and grain boundaries as defects play a key role in determining the dielectric behavior of a material [6]. As the charge carriers reach the grain boundaries and accumulate at the interfaces, they result in net polarization. But as the frequency of the applied field increases, the charge carriers begin to reverse the direction of their movement more often. Therefore, the probability of electrons reaching the grain boundary decreases which leads to a decrease in polarization. Therefore, ε′ decreases with increasing the frequency where all the plots shown in Fig. 6. merge in the high frequency region irrespective of temperature.

3.3.2. The imaginary part of dielectric constant (ε′′) "dielectric loss"

The dielectric loss factor (ε″) can be calculated by using the following equation:

$$\varepsilon'' = \varepsilon'\ Tan\ \delta \qquad (13)$$

Dielectric loss is the energy loss in form of heat into the dielectric material at varying the applied electric field. Relaxation polarization and conduction loss are the two main loss mechanisms that may dissipate energy within a dielectric material.

Fig. 7. shows the frequency and temperature dependency of the dielectric loss (ε") for the pure CuO NPs. The value of dielectric loss (ε") increases with increasing the temperature and decreases with increasing the frequency. When the temperature increases, the conductivity increases and hence the dielectric loss, which is mainly due to the conductivity loss, increases. The large value of the dielectric loss, especially at low frequencies, also can be related to the relaxation polarization that arises from the direct rotation of the dipoles under the applied electric field

(rotational polarization) and movement of charge carriers that accumulates at the interface resulting in an additional electric field which distorts the externally applied electric field (space charge polarization) [17]. This results in a highly resistant grain boundary that requires more energy to exchange charge carriers, and thus the energy loss is high. On the contrary, at high frequency, there are highly conductive grain boundaries that consume a small amount of energy, and therefore, the amount of energy loss is reduced [18].

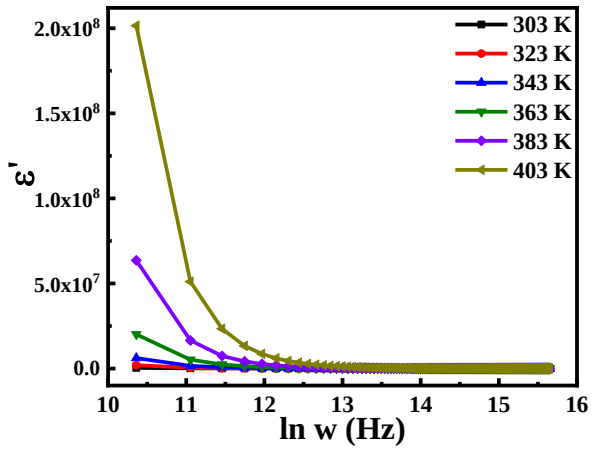

Figure 7. The variation of ε″ with ln (ω) for pure CuO sample at different temperatures.

4 Conclusions

In this work, pure CuO NPs are successfully prepared by hydrothermal method without any surfactant. The NPs have single phase monoclinic structure and a large degree of similarity is found between their morphology. The DC conductivity increases with temperature in a typical semiconducting behavior. The AC conductivity (σ_{AC}) also increases with frequency in the high frequency region while it remains frequency independent in the low frequency region due to the DC conductivity contribution (σ_{DC}). The correlated Barrier Hopping (CBH) model matches well with the AC conductivity behavior. The dielectric constant increases with temperature, particularly at low frequencies due to the orientational and space charge polarizations. Large dispersion of dielectric loss is observed at lower frequencies, which is greatly enhanced when the temperature is raised. The increase in conductivity with temperature indicates that the dielectric loss in the NPs is mainly due to the conduction losses. The obtained properties suggest that the synthesized CuO nanostructures are promising candidate for using in gas sensors and energy storage devices.

5 References

[1] Choi, K. J. and H. W. Jang, One-dimensional oxide nanostructures as gas-sensing materials: review and issues. Sensors, 2010. 10(4): p. 4083-4099.

[2] Zhang, X., et al., High-power and high-energy-density flexible pseudocapacitor electrodes made from porous CuO nanobelts and single-walled carbon nanotubes. ACS nano, 2011. 5(3): p. 2013-2019.

[3] Im, M., et al., New lead-free piezoelectric thin film fabricated using metal-oxide nanosheets at low temperature. Ceramics International, 2019. 45(17): p. 21773-21780.

[4] Sreeju, N., A. Rufus, and D. Philip, Nanostructured copper (II) oxide and its novel reduction to stable copper nanoparticles. Journal of Physics and Chemistry of Solids, 2019. 124: p. 250-260.

[5] Islam, M.R., et al., Effect of Al doping on the structural and optical properties of CuO nanoparticles prepared by solution combustion method: Experiment and DFT investigation. Journal of Physics and Chemistry of Solids, 2020. 147: p. 109646.

[6] Oruç, Ç. and A. Altındal, Structural and dielectric properties of CuO nanoparticles. Ceramics international, 2017. 43(14): p. 10708-10714.

[7] Cheedarala, R.K. and J.I. Song, Face-centred cubic CuO nanocrystals for enhanced pool-boiling critical heat flux and higher thermal conductivities. International Journal of Heat and Mass Transfer, 2020. 162: p. 120391.

[8] Chand, P. and P. Kumar, Effect of precursors medium on structural, optical and dielectric properties of CuO nanostructures. Optik, 2018. 156: p. 743-753.

[9] Hu, Z., et al., CuO@ NiCoFe-S core–shell nanorod arrays based on Cu foam for high performance energy storage. Journal of Colloid and Interface Science, 2021. 599: p. 34-45.

[10] Ao, Y., et al., Preparation and characterization of hierarchical nanostructures composed by CuO nanowires within directional microporous Cu. Vacuum, 2020. 182: p. 109774.

[11] Baghdadi, N., et al., Controlled nanostructuring via aluminum doping in CuO nanosheets for enhanced thermoelectric performance. Journal of Alloys and Compounds, 2021. 869: p. 159370.

[12] Liu, K., et al., A comparative study on the magnetic properties of Fe-doped CuO nanopowders prepared by sol–gel and co-precipitation method. Materials Letters, 2010. 64(2): p. 192-194.

[13] Jagadale, S., et al., Functionalized crown ether assisted morphological tuning of CuO nanosheets for electrochemical supercapacitors. Journal of Electroanalytical Chemistry, 2018. 816: p. 99-106.

[14] Li, S., et al., One-step hydrothermal synthesis of CuO hollow spheres with high photocatalytic activity. Physica E: Low-dimensional Systems and Nanostructures, 2021. 126: p. 114489.

[15] Kumar, P., et al., Band gap tailoring of cauliflower-shaped CuO nanostructures by Zn doping for antibacterial applications. Journal of Alloys and Compounds, 2020. 832: p. 154968.

[16] Othman, A., et al., Influence of Cu doping on structural, morphological, photoluminescence, and electrical properties of ZnO nanostructures synthesized by ice-bath assisted sonochemical method. Journal of Alloys and Compounds, 2016. 683: p. 399-411.

[17] Abdelfatah, M., et al., Fabrication and characterization of flexible solar cell from electrodeposited Cu2O thin film on plastic substrate. Solar Energy, 2015. 122: p. 1193-1198.

[18] Zhang, C., et al., Metal oxide semiconductors with highly concentrated oxygen vacancies for gas sensing materials: A review. Sensors and Actuators A: Physical, 2020. 309: p. 112026.

[19] Abraham, N. and S. Aseena, Dielectric studies of CuO-ZnO heterojunction nanocomposites synthesized by co-precipitation method. Materials Today: Proceedings, 2021. 43: p. 3698-3700.